Author(s): Lehikoinen, Antti & Chiodetto, Nicola & Lantto, Erkki & Arkkio, Antero & Belahcen, Anouar

Title: Monte Carlo Analysis of Circulating Currents in Random-Wound Electrical Machines

Year: 2016

Version: Post print

Please cite the original version:

Lehikoinen, Antti & Chiodetto, Nicola & Lantto, Erkki & Arkkio, Antero & Belahcen, Anouar. 2016. Monte Carlo Analysis of Circulating Currents in Random-Wound Electrical Machines. IEEE Transactions on Magnetics. 12. 0018-9464 (printed). DOI: 10.1109/tmag.2016.2535332.

Monte Carlo Analysis of Circulating Currents in Random-Wound Electrical Machines

Antti Lehikoinen[1], Nicola Chiodetto[1,2], Erkki Lantto[3], Antero Arkkio[1], and Anouar Belahcen[1]
[1]Aalto University, Dept. of Electrical Engineering and Automation, P.O. Box 13000, FI-00076 Espoo, Finland
[2]University of Padova, Electric Drives Lab., Dept. of Industrial Engineering, Via Gradenigo 6a, 35131 Padova, Italy
[3]Sulzer Pumps Finland Oy, Kotka, Finland

Electrical machines with stranded random windings often suffer from considerable circulating current losses. These losses have been poorly studied because of the difficulty and computational cost of modelling stranded windings, and the stochastic nature of the problem due to the uncertain positions of the strands. This paper proposes two methods to model random stranded windings of arbitrary complexity. Firstly, a circuit model considering the entire main flux path is presented, and some practical implementation considerations are discussed. Secondly, a computationally efficient finite element approach based on non-conforming meshing is presented. Finally, a method is proposed to model the random packing process of strands within a slot, without any re-meshing or inductance re-calculation required. The proposed methods are then compared to special no-rotor measurement data of a large number of high-speed induction machines, and a good agreement is observed.

***Index Terms*—Approximation methods, circulating currents, eddy currents, proximity effects, stochastic analysis.**

I. Introduction

HIGH-speed electrical machines often utilize stranded windings, where the large solid conductors are replaced by a number of smaller parallel-connected sub-conductors called strands. This approach is mainly adopted to limit the skin effect losses while maintaining the copper area and the number of turns per slot. However, it can also result in uneven total current distribution between the strands. This phenomenon is called the *circulating current* effect, and has doubled the resistive stator losses in some high-speed machines [1].

Most analysis on AC resistive losses has mainly focused on the skin and proximity effect losses, related to the uneven current density distribution *within* each conductor. For machines with form-wound windings with relatively large solid conductors both analytical [2] and finite element (FE) [3]–[7] models have been utilized. Windings consisting of a larger number of thinner conductors, usually in the form of idealized Litz wires, have often been FE analysed by homogenization in either frequency- or time-domain or both [8]–[14]. Some analytical approaches have also been published, along with a few brute-force studies [15]–[18].

By contrast, research specifically on circulating currents in stranded windings has been scarce. Both FE-based [3], [7], [19]–[21] and analytical [22], [23] approaches have largely focused on form-wound windings, with the circulating currents often effectively suppressed by conductor transpositions. Nevertheless, a few more relevant papers were published recently. In 2014 and 2015, two circuit-based models were used to analyse permanent magnet (PM) machines [24], [25]. Furthermore, in 2015 a computationally light method for FE analysis of arbitrary windings was proposed [26], [27].

None of the listed publications has considered truly *random*-wound windings. Instead, the configuration of strands inside the slots has been assumed known and deterministic. Therefore, this paper proposes two methods to analyse the statistical properties of circulating currents. Firstly, the circuit model in [24] is extended to take also the rotor of the machine into account. Secondly, the FE approach of [27] is improved. Furthermore, practical software implementation of the methods is discussed. Finally, an approach is proposed to approximately model the uncertain winding process, with no re-meshing or inductance re-calculation required.

The methods are then used in conjunction with the Monte Carlo (MC) method to model a special no-rotor test set-up of high-speed induction machines, and the simulation results are compared to measurement data. A good match is obtained between the simulations and measurements. The full-load behaviour of the machines predicted by the computational model is then briefly analysed, although further work will still be needed to fully validate the methods in these conditions.

II. Circulating Current Phenomenon

In many electrical machines, the stator winding is composed of a large number of thin sub-conductors connected in parallel. This kind of winding is usually called *stranded*, and the sub-conductors respectively *strands*. When the sub-conductors have a non-rectangular cross-section the winding can also be called *random-wound*, due to the fact that the exact positions of the conductors inside slots cannot be precisely controlled. This uncertainty in positioning is by the fact that semi-closed

Manuscript received December 10, 2015; revised February 2, 2016; accepted February 21, 2016. Date of publication 2016; date of current version 2016. Corresponding author: A. Lehikoinen (email: antti.lehikoinen@aalto.fi). Color versions of one or more of the figures in this paper are available online at http://ieeexplore.ieee.org.
Digital Object Identifier 10.1109/TMAG.2016.2535332

slots are often utilized in high-speed machines, requiring the strands to be inserted into the slots a few at a time [28].

Due to the slot flux, each strand will see a different flux linkage and thus have a different inductance. This often leads to a difference in the total current of each parallel current path, increasing the total resistive losses. The difference between the individual and average strand currents is called the circulating current, and the associated losses the circulating current losses respectively.

If the skin and proximity effect losses are neglected, the circulating current losses P_{cc} can be obtained with

$$P_{\mathrm{cc}} = P_{\mathrm{AC}} - P_{\mathrm{DC}}, \tag{1}$$

where P_{AC} denotes the actual resistive losses, whereas P_{DC} are the ideal resistive losses from the DC approximation. However, a more practical indicator will often be the *circulating current factor* k_{cc}, i.e. the ratio between P_{AC} and P_{DC}. For each parallel path l, k_{cc}^l can be obtained with

$$k_{\mathrm{cc}}^l = \frac{P_{\mathrm{cc}}^l + P_{\mathrm{DC}}^l}{P_{\mathrm{DC}}^l} = \frac{\sum\limits_{i\in l} |\mathbf{i}_i|^2}{\frac{1}{N_{\mathrm{p}}} \left| \sum\limits_{i\in l} \mathbf{i}_i \right|^2}, \tag{2}$$

where N_{p} is the number of parallel strands in the path, and the vector $\mathbf{i}$ contains all linearly independent strand currents [1]. The latter form of (2) has the benefit of remaining valid even with the skin and proximity effect losses taken into account. Equation (2) can be extended for phases and the entire machine in a similar fashion.

In the following two sections, two methods are proposed to analyse the circulating current phenomenon. First, an equivalent circuit based model is presented, also taking into account the effect of the rotor circuit. After that, a computationally efficient FE model is presented.

III. Circuit Model

Throughout this paper, the following notation will be used. $\mathbf{I}$, $\mathbb{1}$, and $\mathbf{0}$ are used to denote the identity matrix and matrices of all ones and zeros, respectively. If necessary, the size of a matrix will be expressed in the subscript, for instance $\mathbb{1}_{r\times 1}$ denoting an all-one column vector of r entries. Furthermore, the term *strand* is used to denote a single sub-conductor in a single slot, unless otherwise specified.

The analytical circulating current model proposed in [24] is briefly re-presented here, and generalized to cover arbitrary circuit topologies. The leakage flux of a single slot of a machine is considered first. If there are n strands in the slot with currents i, the voltages u over the strands (between the ends of the machine) can be obtained from

$$\begin{aligned} u_1 &= r_1 i_1 + \mathrm{j}\omega \left(L_1 i_1 + M_{12} i_2 + \dots M_{1n} i_n \right) \\ u_2 &= r_2 i_2 + \mathrm{j}\omega \left(M_{21} i_1 + L_2 i_2 + \dots M_{2n} i_n \right) \\ &\vdots \\ u_n &= r_n i_n + \mathrm{j}\omega \left(M_{n1} i_1 + \dots M_{n(n-1)} i_{n-1} + L_n i_n \right), \end{aligned} \tag{3}$$

where r are the strand resistances, and L and M the self and mutual (leakage) inductances respectively. It should be noted that the term *inductance* is maybe used in a somewhat non-standard fashion here, and should be understood as the ratio between the current flowing in a single strand of the machine and the voltage induced over it or some other strand. The inductances can be calculated with analytical methods of varying complexity [29]–[31], or extracted from FE analysis [32], [33].

The situation is slightly more complicated in an actual machine. Firstly, there are several slots, each of them governed by equations like (3). Also, the main flux of the machine will induce a significant electromotive force (emf) on the strands, referred to as *back-emf* in this paper. Thus, for each slot k it can be written

$$\mathbf{u}_{\mathrm{slot},k} = \left(\mathbf{R}_k + \mathrm{j}\omega \mathbf{L}_k \right) \mathbf{i}_{\mathrm{strand},k} + \mathbf{E}_k. \tag{4}$$

Here $\mathbf{R}$ and $\mathbf{L}$ are the slot resistance and inductance matrices with entries corresponding to (3). $\mathbf{E}$ is the vector of back-emfs induced in the strands.

In most machines, the majority of the main flux will travel along the teeth of the machine, rather than the slots. Thus, the same back-emf will be induced on all strands in the same slot. An important exception are e.g. permanent magnet machines with open slots [34]. However, this paper will deal mainly with high-speed machines with semi-closed slots, so the coupling between the circulating currents and main flux should be weak.

Secondly, not all strands in the machine are typically in parallel. Instead, several strands may be connected in series, in one or more slots. Thus, the number of independent currents is often significantly smaller than the total number of strands in the machine. By utilizing e.g. the loop method, these independent currents $\mathbf{i}$ can be determined, and the strand currents then expressed as

$$\mathbf{i}_{\mathrm{strand},k} = \mathbf{C}_k \mathbf{i}. \tag{5}$$

The loop matrix $\mathbf{C}_k$ has the entries

$$[\mathbf{C}_k]_{i,j} = \begin{cases} 1, & \text{current } j \text{ flows forwards in strand } i \text{ of slot } k \\ -1, & \text{current } j \text{ flows backwards in strand } i \text{ of slot } k \\ 0, & \text{otherwise.} \end{cases} \tag{6}$$

The *forward* and *backward* directions can be freely chosen, as long as they are consistent.

Finally, the total supply voltage for each current path has to equal the sum of all Q_{s} slot voltages of the path, i.e.

$$\begin{aligned} \mathbf{u}_{\mathrm{supply}} &= \sum_{k=1}^{Q_{\mathrm{s}}} \mathbf{C}_k^{\mathrm{T}} \mathbf{u}_{\mathrm{slot},k} \\ &= \sum_{k=1}^{Q_{\mathrm{s}}} \mathbf{C}_k^{\mathrm{T}} \left(\mathbf{R}_k + \mathrm{j}\omega \mathbf{L}_k \right) \mathbf{C}_k \mathbf{i} + \mathbf{C}_k^{\mathrm{T}} \mathbf{E}_k. \end{aligned} \tag{7}$$

The currents $\mathbf{i}$ – and by extension the actual strand currents (5) – can now be easily solved. Resistive losses can then be obtained from the strand currents and resistances.

A. Practical Matrix Assembly

While (7) is fully sufficient to cover any stator winding configuration, forming all the per-slot matrices $\mathbf{C}_k$ by hand would be very cumbersome and error-prone. Thus, a systematic, easy-to-implement approach is briefly presented here for typical windings. A Delta-connected three-phase machine with a two-layered winding and two parallel paths is used as an example, due to a similar one appearing later in the results section.

Firstly, the vector $\mathbf{u}_{\text{supply}}$ of supply voltages of each current path can be obtained by repeating the line voltages as

$$\begin{aligned}\mathbf{u}_{\text{supply}} &= \begin{bmatrix} \mathbb{1}_{2N_\text{p}\times 1} & \mathbf{0} & \mathbf{0} \\ \mathbf{0} & \mathbb{1}_{2N_\text{p}\times 1} & \mathbf{0} \\ \mathbf{0} & \mathbf{0} & \mathbb{1}_{2N_\text{p}\times 1} \end{bmatrix} \mathbf{u}_{\text{line}} \\ &= \left(\mathbf{I}_{3\times 3} \otimes \mathbb{1}_{N_\text{p}\times 1}\right) \mathbf{u}_{\text{line}}. \end{aligned} \tag{8}$$

Here, $\mathbf{u}_{\text{line}}$ is the vector of line voltage phasors

$$\mathbf{u}_{\text{line}} = \begin{bmatrix} \underline{u}_1 & \underline{u}_2 & \underline{u}_3 \end{bmatrix}^\text{T}. \tag{9}$$

On the second row of (8), a Kronecker product notation has been introduced both for compactness and simplicity of implementation in any high-level programming language.

Likewise, the loop matrices $\mathbf{C}$ can be partitioned into blocks based on the number of phases, parallel paths and winding layers. For instance, if slot 1 were to host the positive coil side of path 1 and the negative coil side of path 2 in its upper and lower layers respectively, $\mathbf{C}_1$ could be written as

$$\begin{aligned}\mathbf{C}_1 &= \begin{bmatrix} \mathbf{C}^\text{b} & \mathbf{0} & \mathbf{0} & \mathbf{0} & \mathbf{0} & \mathbf{0} \\ \mathbf{0} & -\mathbf{C}^\text{b} & \mathbf{0} & \mathbf{0} & \mathbf{0} & \mathbf{0} \end{bmatrix} \\ &= \begin{bmatrix} 1 & 0 & 0 & 0 & 0 & 0 \\ 0 & -1 & 0 & 0 & 0 & 0 \end{bmatrix} \otimes \mathbf{C}^\text{b} = \mathbf{F}_1 \otimes \mathbf{C}^\text{b}. \end{aligned} \tag{10}$$

Here, two new matrix types ($\mathbf{C}^\text{b}$ and $\mathbf{F}_k$) were introduced. They will be described next.

$\mathbf{C}^\text{b}$ is used to describe the basic strand configuration per layer. Of course, the necessary assumption for its use is that the configuration does not change from layer to layer, or slot to slot. Assuming – for now – also that all strands in the same turn are close to each other, $\mathbf{C}^\text{b}$ can be written as

$$\mathbf{C}^\text{b} = \mathbb{1}_{N_\text{turns}\times 1} \otimes \mathbf{I}_{N_\text{p}\times N_\text{p}}. \tag{11}$$

N_turns is the number of turns per layer.

The second new matrix $\mathbf{F}_k$, on the other hand, describes which parallel paths traverse the slot k, and to which direction. Each $\mathbf{F}_k$ can be constructed as follows. Let $\widetilde{\mathbf{F}}$ be a $2 \times Q_\text{s}$ matrix describing the overall winding configuration of the machine, with the entries

$$\left[\widetilde{\mathbf{F}}\right]_{i,k} = \begin{cases} j & \text{parallel path } j \text{ has a positive coil side} \\ & \text{in the } i^\text{th} \text{ layer of slot } k \\ -j & \text{parallel path } j \text{ has a negative coil side} \\ & \text{in the } i^\text{th} \text{ layer of slot } k. \end{cases} \tag{12}$$

Parallel paths 1 and 2 are assumed to belong to phase a of the machine, paths 3 and 4 to phase b, and similarly for phase c. Then, each $\mathbf{F}_k$ can be obtained from $\widetilde{\mathbf{F}}$ by setting

$$\left[\mathbf{F}_k\right]_{i,j} = \begin{cases} \text{sign}\left(\left[\widetilde{\mathbf{F}}\right]_{i,k}\right), & \text{if abs}\left(\left[\widetilde{\mathbf{F}}\right]_{i,k}\right) = j \\ 0, & \text{otherwise.} \end{cases} \tag{13}$$

Even $\widetilde{\mathbf{F}}$ can be constructed in a simple fashion. For a typical diamond winding configuration it is sufficient to first calculate

$$\widetilde{\mathbf{F}} = \begin{bmatrix} 1 & -5 & 3 & -2 & 6 & -4 \\ 2 & -6 & 4 & -1 & 5 & -3 \end{bmatrix} \otimes \mathbb{1}_{1\times q}. \tag{14}$$

In other words, the typical phase belt order in the rotation direction is first manually written for both layers. Then, each entry of the 2×6 matrix is replicated column-wise to correspond to the number of slots per pole and phase q. If necessary, short-pitching can then be modelled by shifting the entries of the upper row of (14) to correspond to the pole pitch of the machine.

B. Taking the Rotor into Account

In [24], the back-EMF vector $\mathbf{E}$ was assumed to be only due to permanent magnet flux, and equal for all the strands in the same slot. Thus, $\mathbf{E}$ could be written as

$$\mathbf{E}_k = \text{j}\omega r_\delta l_\text{eff} \exp\left(\text{j}\frac{2\pi}{Q_\text{s}}k\right) B \cdot \mathbb{1}_{N_\text{strands}\times 1}, \tag{15}$$

where l_eff and r_δ are the effective length and air-gap radius of the machine, respectively. B is the amplitude of the fundamental air-gap flux density.

However, B will also depend on the currents of the machine, especially in an induction machine with a small air-gap. Thus, (15) cannot be used directly. Therefore, an approach is proposed to take both the magnetizing and rotor branch into account in the circuit model, based on the well-known T equivalent circuit of an induction machine. Obviously, it is assumed that the circulating current phenomena do not significantly distort the air-gap flux density, so that the basic space vector approximation remains valid. Then, the relationship

$$B = k_\text{B}\underline{i}_\text{m} = k_\text{B}(\underline{i}_\text{s} + \underline{i}_\text{r}) \tag{16}$$

can be established between B and the magnetizing current vector $\underline{i}_\text{m}$. The coefficient k_B can be derived analytically based on the machine geometry, or obtained from finite element analysis. A method utilizing the concepts derived in this paper is presented in Appendix A.

To determine the rotor current space vector $\underline{i}_\text{r}$, the rotor branch voltage equation

$$0 = \text{j}\omega L_\text{m}\left(\underline{i}_\text{s} + \underline{i}_\text{r}\right) + \left(\frac{R_\text{r}}{s} + \text{j}\omega L_{\sigma\text{r}}\right)\underline{i}_\text{r} \tag{17}$$

has to be added to the model. The stator current vector $\underline{i}_\text{s}$, on the other hand, can be obtained directly from the stator loop currents $\mathbf{i}$ by

$$\underline{i}_\text{s} = \mathbf{P}_{\alpha\beta}\mathbf{L}_\text{I}\mathbf{i}. \tag{18}$$

Here, the matrices

$$\begin{aligned}\mathbf{L}_\text{I} &= \mathbf{I}_{3\times 3} \otimes \mathbb{1}_{1\times 2N_\text{p}} \\ \mathbf{P}_{\alpha\beta} &= \frac{2}{3}\begin{bmatrix} 1 & \exp\left(\text{j}\frac{2\pi}{3}\right) & \exp\left(\text{j}\frac{4\pi}{3}\right) \end{bmatrix} \end{aligned} \tag{19}$$

are used to calculate the phase currents from the loop currents $\mathbf{i}$, and the current space vector from the phase currents, respectively.

With this notation, the final system of equations to be solved can be written as

$$\mathbf{u}_{\text{supply}} = \sum_{k=1}^{Q_\text{s}} \mathbf{C}_k^\text{T} \left(\mathbf{R}_k + \text{j}\omega\mathbf{L}_k\right)\mathbf{C}_k\mathbf{i} + \mathbf{C}_k^\text{T}\widetilde{\mathbf{k}}_k\left(\mathbf{P}_{\alpha\beta}\mathbf{L}_\text{I}\mathbf{i} + \underline{i}_\text{r}\right)$$
$$0 = \text{j}\omega L_\text{m}\left(\mathbf{P}_{\alpha\beta}\mathbf{L}_\text{I}\mathbf{i} + \underline{i}_\text{r}\right) + \left(\frac{R_\text{r}}{s} + \text{j}\omega L_{\sigma\text{r}}\right)\underline{i}_\text{r}. \quad (20)$$

The new short-hand coefficient

$$\widetilde{\mathbf{k}}_k = \frac{\mathbf{E}_k}{\underline{i}_\text{m}} = \text{j}\omega r_\delta l_\text{eff}\text{exp}\left(\text{j}\frac{2\pi}{Q_\text{s}}k\right)k_\text{B}\cdot\mathbb{1}_{N_\text{strands}\times 1}, \quad (21)$$

describing the ratio between $\mathbf{E}$ and $\underline{i}_\text{m}$ has been adopted for clarity, obtained from (16) and (15).

IV. Finite Element Model

Finite element modelling of circulating current problems has been notoriously difficult due to the excessively dense mesh required for representing the stranded conductors, and the large number of strand voltages to be solved [7]. This paper proposes an approach to tackle these two problems. Analysis is limited to linear time-harmonic 2D problems, although extension to the time-domain with nonlinearities, or three dimensions should be relatively straightforward.

A solution to the dense mesh problem was proposed in in [26], [27], based on non-conforming meshing around the conducting domains. The method was then successfully used to simulate a simplified PM machine in the time-domain. However, even with this method the number of unknown strand voltages could be uncomfortably large – easily in excess of 10 000 in a realistic problem with the entire cross-section of the machine simulated.

Thus, the method is slightly modified here. Assuming that the current density inside each strand is almost uniform, the governing equation for the Galerkin-discretized vector potential $\mathbf{a}$ is

$$\mathbf{S}\mathbf{a} + \sum_{k=1}^{Q_\text{s}}\mathbf{F}_k\mathbf{i}_{\text{strand},k} = \mathbf{0}, \quad (22)$$

where $\mathbf{S}$ is the typical FE stiffness matrix [32]. The current source matrix $\mathbf{F}$ has the entries

$$\left[\mathbf{F}_k\right]_{i,j} = \frac{\int_{D_{k,j}}\varphi_i\,\text{d}S}{|D_{k,j}|}, \quad (23)$$

where $D_{k,j}$ is the domain of the j^th strand of slot k, and $|D_{k,j}|$ its cross-sectional area. Shape functions are denoted by φ. Based on the point-source approach in [27], $\mathbf{F}$ can be approximated by

$$\left[\mathbf{F}_k\right]_{i,j} \approx \begin{cases} \varphi_i\left(\mathbf{x}_{k,j}^\text{c}\right), & \mathbf{x}_{k,j}^\text{c}\in D_{k,j} \\ 0, & \text{otherwise,}\end{cases} \quad (24)$$

where $\mathbf{x}_{k,j}^\text{c}$ is the center point of the strand j in slot k. This way, the strands can be completely ignored while meshing the slot regions, yielding a huge reduction in the number of nodes.

On the other hand, since the back-emf induced in one particular strand l of slot k is

$$E_{k,l} = \text{j}\omega l_\text{eff}\frac{1}{|D_{k,j}|}\int_{D_{k,l}} A\left(\mathbf{x}\right)\,\text{d}S, \quad (25)$$

the vector of back-emfs for this slot can be obtained from

$$\mathbf{u}_{\text{slot},k} = \text{j}\omega l_\text{eff}\mathbf{F}_k^\text{T}\mathbf{a}. \quad (26)$$

Then, combining (22) to the circuit equations presented earlier yields the matrix system

$$\begin{bmatrix} \mathbf{S} & \sum_{k=1}^{Q_\text{s}}\mathbf{F}_k\mathbf{C}_k \\ \text{j}\omega l_\text{eff}\sum_{k=1}^{Q_\text{s}}\mathbf{C}_k^\text{T}\mathbf{F}_k & \sum_{k=1}^{Q_\text{s}}\mathbf{C}_k^\text{T}\mathbf{R}_k\mathbf{C}_k \end{bmatrix}\begin{bmatrix}\mathbf{a}\\ \mathbf{i}\end{bmatrix} = \begin{bmatrix}\mathbf{0}\\ \mathbf{u}_\text{supply}\end{bmatrix}. \quad (27)$$

This system can then be further modified to include e.g. permanent magnets or a rotor cage to the analysis. For this purpose, any well-established FE approach can be used.

V. Modelling Randomness

The analysis presented so far has assumed that the strand configuration is known in each slot. However, in a random-wound machine – as the name suggests – the configuration will usually vary from slot to slot, and machine to machine in a stochastic fashion. Although some preliminary attempts have been made to include such geometric uncertainty into the model [35], Monte Carlo analysis will be utilized in this paper. Thus, a method is needed to generate samples from the random strand configurations.

There are extremely many ways to pack the strands inside one slot. However, in this paper it is assumed that the randomness can be satisfyingly modelled by swapping the positions of the strands with each other, rather than re-packing them. In other words, a single feasible packing is first generated, and the positions of strands in that configuration are numbered and stored. Then, the indexing of the strands – which strand gets assigned to which position – within the pre-defined packing is randomly permuted. A brief justification for this assumption can be found in Appendix B. An example of a packing – also used later in the results section – with a filling factor of 0.37 is illustrated in Fig. 1.

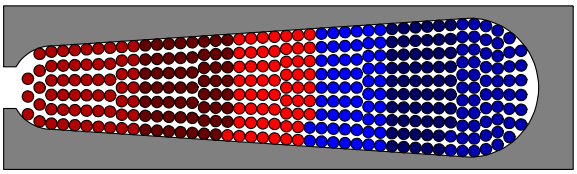

Fig. 1. The packing of strands used in the simulations. Winding layers are illustrated with the red and blue colors, while different shades are used for turns.

This randomization of strand indices is equivalent to randomly permuting the rows and columns of the resistance and inductance matrices by assigning

$$\mathbf{L} := \mathbf{P}^\text{T}\left(\theta\right)\mathbf{L}\mathbf{P}\left(\theta\right). \quad (28)$$

Here, $\mathbf{P}\left(\theta\right)$ is a random permutation matrix with a suitable probability density function (pdf), and θ is used to denote the outcome in the probability space. Based on 7, this permutation approach can also be understood as a permutation of the rows of the loop matrices, by

$$\mathbf{C}_k := \mathbf{P}\left(\theta\right)\mathbf{C}_k. \quad (29)$$

In double layer machines, there is usually a thick layer of insulation between the layers. Thus, it can be reasonably assumed that the strands will not travel from layer to layer, and $\mathbf{P}(\theta)$ can thus be written with two smaller block permutation matrices $\mathbf{P}_1, \mathbf{P}_2$ as

$$\mathbf{P}(\theta) = \begin{bmatrix} \mathbf{P}_1(\theta) & \mathbf{0} \\ \mathbf{0} & \mathbf{P}_2(\theta) \end{bmatrix}. \tag{30}$$

The permutation procedure is illustrated in Fig. 2, where the indices of the first six strands $(1 \dots 6)$ have been flipped $(6 \dots 1)$. In this case, the upper-left 6×6 block of the permutation matrix would be the so-called exchange matrix, i.e. a matrix with ones on the counter-diagonal (running from the lower left to the upper right corner).

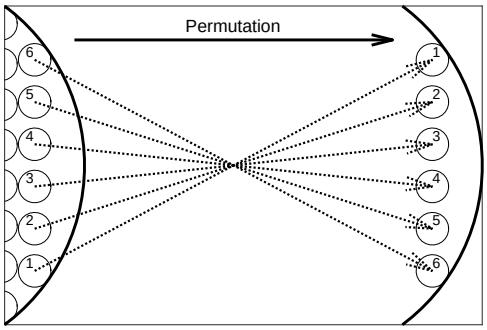

Fig. 2. An illustration of a permutation of six strands at the slot bottom.

This approach has two important benefits. Firstly, the mathematically difficult random packing problem has been reduced to generating random permutations. Also, it is now possible to utilize pre-calculated slot matrices ($\mathbf{L}$ or $\mathbf{F}$), instead of having to assemble new ones for each Monte Carlo sample. The method could possibly also be classified as a Quasi-Monte Carlo method, since only a structured subset of the entire probability space is explored.

A. Generating Permutations

Obviously, the distribution of $\mathbf{P}$ should be known, and a method to draw samples from this distribution is needed. Since no measured data directly related to strand positioning is available, the following assumption is made. Let $\mathbf{x}_k^0$ be the positions in the pre-defined packing, and d_{ij} be the distance

$$d_{ij} = \|\mathbf{x}_i^0 - \mathbf{x}_j^0\|. \tag{31}$$

Then, the probability that strand i gets assigned to position j (i.e. the only non-zero entry on row i of $\mathbf{P}$ is on column j) is assumed to approximately follow the discrete normal-like distribution

$$\begin{aligned} p_i(j) &= \Pr\left(\text{strand } i \text{ assigned to } \mathbf{x}_j^0\right) \\ &= \Pr\left([\mathbf{P}]_{ij} = 1\right) \sim \frac{1}{c}\exp\left(-\frac{d_{ij}^2}{2\sigma^2}\right). \end{aligned} \tag{32}$$

The normalization coefficient c can be ignored, since it will not be required by the algorithm proposed shortly. The variation parameter σ defines how far the strands are expected to stray from their default positions. For further use, the per-unit notation

$$\sigma_{\text{pu}} = \frac{\sigma}{\max d_{ij}} \tag{33}$$

is adopted for clarity.

Generating random permutations from a distribution other than the uniform one is a nontrivial task. In this case, even defining the pdf of $\mathbf{P}$ in such a way that (32) holds is not straightforward. Nevertheless, Fig. 3 shows an approximative Gibbs-inspired algorithm for generating samples of $\mathbf{P}$, that was observed to yield satisfactory results based on extensive numerical analysis.

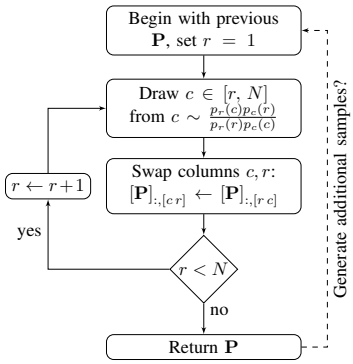

Fig. 3. A sampling algorithm for generating random permutations.

Indeed, an example with 174 strands and $\sigma_{\text{pu}} = 0.2$ can be seen in Fig. 4. The probabilities of the strands 1 and 100 ending up in the positions $1 \dots 174$ are shown. The solid lines have been estimated from 30 000 samples to eliminate most noise, while the dotted lines correspond to the now-normalized target distribution (32). It can be seen that the sampling algorithm produces permutation matrices with properties reasonably close to the desired ones, considering that (32) is already highly approximative of the real physical phenomenon.

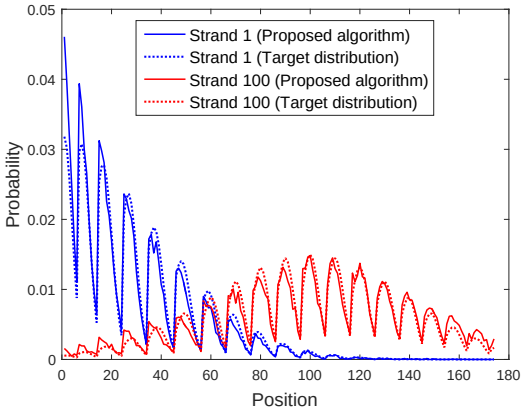

Fig. 4. Example of permutations generated by proposed the algorithm, and the target distribution.

VI. Simulation and Measurement Results

For evaluating the proposed methods, winding-related measurement data was provided by a manufacturer of high-speed

2-pole solid-rotor induction machines in the 200 kW range, with the rated frequencies around 450 Hz. Measurements of a total of 230 nominally identical machines of the same product series were analysed. In the tests, the rotors of the machines had been removed to obtain information about the circulating currents in particular. The main dimensions of the machines can be found in Table I, and the slot shape in Fig. 1.

TABLE I
MAIN DIMENSIONS OF MACHINES.

Winding connection
Number of parallel paths
Number of winding layers
Number of turns
Number of strands per slot
Number of stator slots
Coil pitch (slots)
Stator diameter (mm)

The machines had been measured with a dedicated tester, utilizing feedback control to force the machine currents to follow the desired waveforms, also measuring the input current and voltage phasors along with powers [36]. In the tests, balanced sinusoidal currents had been used, with an amplitude of 5 A and frequencies from approximately 15 Hz to 900 Hz. The machines had been delta-connected.

From the measurements, active and reactive input powers were extracted. Core losses were estimated with FEM assuming no circulating currents, ranging approximately 1 to 15 % of the input power in the frequency range [37]. They were then removed from the active power to obtain the total losses in the stator winding. The circulating current losses and factors were finally calculated with (1) and (2).

A. Skin and Proximity Effects

In the tested frequency range, the strand radius was less than 15 % of the skin depth. Thus, the skin and proximity effect losses could reasonably be assumed negligible [11], [12]. Nevertheless, to test this assumption, a brute-force FE simulation at 1 kHz was performed on one slot segment of the machine. The strands were meshed with two layers of elements each to obtain accurate current density distributions [13], [32], resulting in a total of 57 300 elements. The winding configuration was the same as in slot 1 of the actual machine.

The results were then compared to the ones obtained with the approximate FEM model proposed in Section IV. A maximum relative difference of 4.2 % was observed between the total layer currents obtained with the two methods. With the per-layer circulating current coefficients, the error was 2.2 % at most. Although this problem was a simplified one, it did indeed support the assumption that the skin and proximity effects can be safely ignored.

B. Simulation Results with Independent Strand Packings

A simplified version of the test set-up was first modelled with the proposed circuit and FE methods. The machines were supplied with a three-phase delta-connected voltage source. The supply voltages were solved simultaneously with the currents, so that total phase currents with equal magnitudes and exactly 120 degree phase shifts were obtained. Supply cable impedances were assumed zero, and the strand resistances – also taking into account the end-winding length – were estimated analytically. End-winding inductances were ignored, due to their presumably small effect on the circulating currents [38]. Finally, the strand inductances for the circuit model were calculated with FEA, based on the strand packing seen in Fig. 1 [25], [37]. The entire stator bore was meshed in the FE method, and modelled with a small magnetizing inductance in the circuit method. Frequencies up to $1.2 \times f_{\mathrm{N}} = 550$ Hz were analysed.

In the FE model, the total number of unknowns was approximately 12 000. Thus, the direct sparse solver of Matlab could easily be utilized. Obviously, in the circuit model only the currents and supply voltages were solved, resulting in $348 + 3$ unknowns. The total solution time of a single configuration was well under 1 second for both methods.

The uncertainty in the strand configurations was modelled with the Monte Carlo method, by permuting the rows of the loop matrices with the algorithm proposed in Section V-A. The random permutations for each slot and layer were assumed to be independent. The behaviour of each randomized machine was then analysed over the entire frequency range without re-randomization, to simulate the testing process of an actual individual machine. The simulations were then run in parallel on 8 cores. Based on some initial test runs, the number of MC samples was chosen to be 2000 to obtain good convergence at a reasonable computational cost.

The total circulating current factors $k_{\mathrm{cc,tot}}$ as a function of frequency are shown in Figs. 5 and 6, calculated with the circuit and FE model respectively. The solid curves show the simulated mean values with different σ_{pu}, while the corresponding standard deviations are denoted by the vertical error bars. Measured results are shown with the thick black line. Convergence of var $(k_{\mathrm{cc,tot}})$ calculated with the circuit model at three different frequencies can be seen in Fig. 7, with $\sigma_{\mathrm{pu}} = 0.2$. Finally, estimated distributions of total and per-phase k_{cc} at 400 Hz are shown in Figs. 8 and 9.

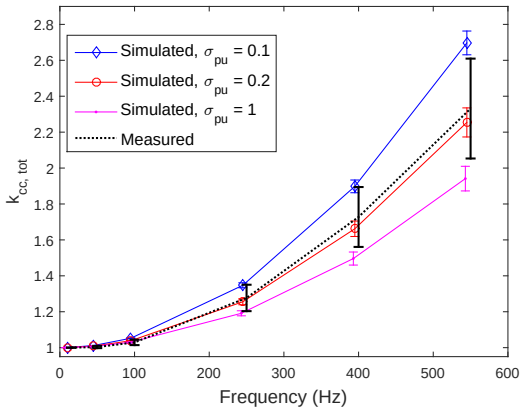

Fig. 5. Total circulating current factors calculated with the circuit model as a function of frequency, with different σ_{pu}.

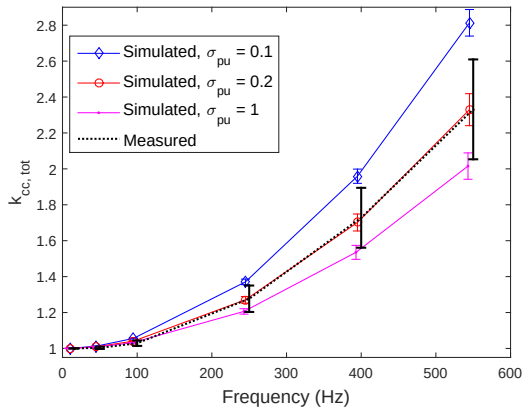

Fig. 6. Total circulating current factors calculated with the FE model as a function of frequency, with different σ_{pu}.

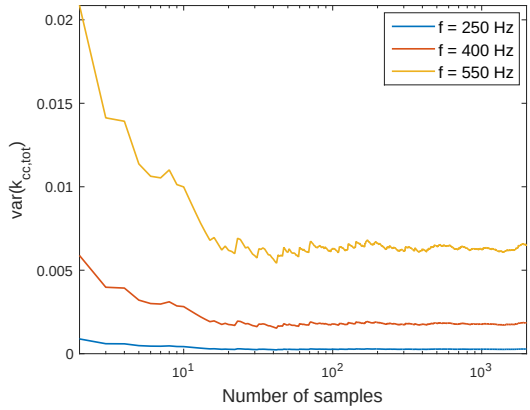

Fig. 7. Convergence of the circulating current factor variance as a function of MC samples, illustrated at three different frequencies.

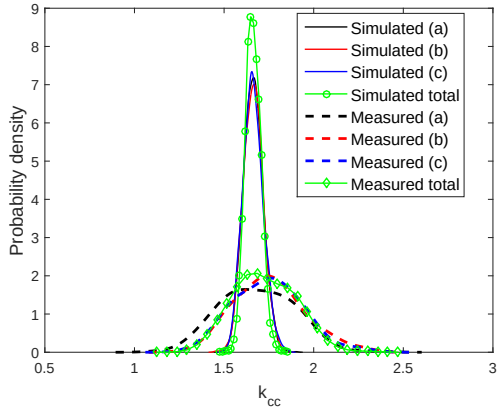

Fig. 8. Probability density functions of the circulating current factors at 400 Hz, with the simulated results calculated by the circuit model at $\sigma_{\text{pu}} = 0.2$. Factors for each phase (a,b,c) and the entire machine are shown.

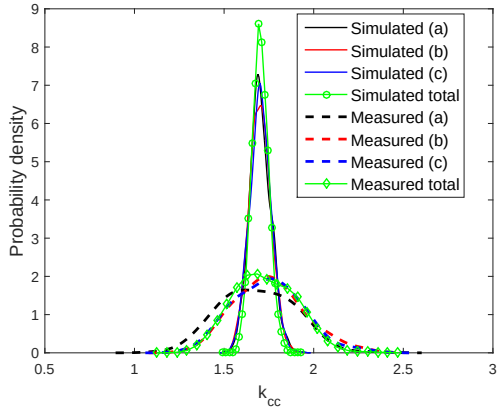

Fig. 9. Probability density functions of the circulating current factors at 400 Hz, with the simulated results calculated by the FE model at $\sigma_{\text{pu}} = 0.2$. Factors for each phase (a,b,c) and the entire machine are shown.

It can be seen that the circuit model and FE model yielded very similar results, with approximately correct mean values at $\sigma_{\text{pu}} = 0.2$. Both the simulated and measured values appear to be normally distributed, but the measured results exhibit significantly higher variance. Furthermore, the simulated per-phase k_{cc} exhibit clearly larger variance than the simulated $k_{\text{cc,tot}}$, whereas the measured values are almost equally distributed. The number of samples used should be sufficient, though, based on Fig. 7.

In an attempt to improve the results, some refinements were then made on the simulation model. The voltage supply was changed to star connection (to comply with the actual test set-up). Also, it was observed that the simulation models underestimated both the total phase resistance and inductance by approximately 8 % and 22 % on low frequencies. These differences could probably be explained by the end-winding impedance, and possibly also the main flux fringing due to the absence of the rotor (increasing the magnetizing inductance). A corresponding correction impedance was then added in series with each parallel path of the machine.

These refinements only resulted in very minor changes from Figs. 5-9, so these results are not shown. Nevertheless, some conclusions can be drawn. Slightly surprisingly, increasing the variation σ_{pu} decreased the mean circulating current losses. This could be easily explained by analysing the assumed winding configuration, though. In Section III-A the per-layer default configuration matrix $\mathbf{C}^{\text{b}}$ was defined so that the strand positions within layer (before randomization) did not change from slot to slot – any strand at the bottom of the layer would be at the bottom of the layer in any slot. This configuration would result in very large circulating current losses. Thus, any change in the configuration would very likely yield lower losses. Indeed, this can be observed from the simulation results as well.

More surprisingly, σ_{pu} did not seem to influence the variance of the circulating current losses. This is slightly paradoxical, since setting σ_{pu} to zero would obviously result in a zero variance in the results. Apparently, the variance would then rise very rapidly before saturating at some $\sigma_{\text{pu}} < 0.1$. This phenomenon is probably related to the extremely large number of possible strand configurations for the entire machine $(174!)^{72}$, resulting in a very low probability of obtaining any outlying results.

C. Simulation Results with Dependent Strand Packings

Since refining the deterministic part of the simulation models did not improve accuracy, it became evident that the approach to model the randomness was probably inaccurate. Thus, the following simple adjustment was made to the MC procedure.

In the first models, the permutation matrices were drawn independently from the same distribution for the entire layer, assuming no large error was caused by this. However, in an actual machine the positions of all strands are probably slightly interdependent, both due to the manufacture process and mechanical reasons as well. Furthermore, the strands of each turn can probably be expected to stay close to each other. A more detailed analysis of the manufacture process and its effect on $\mathbf{P}$ is underway, but for now the following ad-hoc procedure was observed to yield relatively good results.

Indeed, the slots, turns, and parallel paths of the machine were first ordered as seen in Fig. 10. The correspondence between numbering the paths and the phases of the machine has been described in III-A. Then, the strand configurations of each *turn* were randomized in a successive fashion, each based on the preceding turn with the permutation matrix

$$\mathbf{P}_{k+1} = \mathbf{P}\left(\theta\right)\mathbf{P}_k. \tag{34}$$

The random matrices $\mathbf{P}\left(\theta\right)$ were still generated with the same algorithm to be able to adjust the level of slot-to-slot variation. The values of σ were calculated from σ_{pu} separately for each turn with (33). The identity matrix was used as $\mathbf{P}_0$.

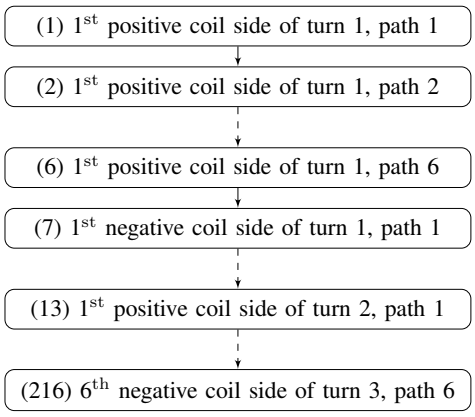

Fig. 10. Ordering of the turns of the machine used with the dependent packing algorithm.

Again, $k_{\text{cc,tot}}$ as a function of frequency can be seen in Fig. 11, and the estimated pdfs (at $\sigma_{\text{pu}} = 0.037$) in Fig. 12. As can be seen, the simulated distribution is now much wider and thus closer to the measured one. Also, the total circulating current factor has a variance close to the per-phase factors, again in agreement with the measured results. FE results were again very similar to the circuit model ones, and are thus not shown.

One very important observation is that significantly smaller values of σ_{pu} were now required to obtain the best agreement with measurements. In other words, very small changes in the strand positions resulted in large variation in the circulating current losses. Indeed, most strands either did not change their relative positions at all from one slot to the next one, or only swapped places with an adjacent strand.

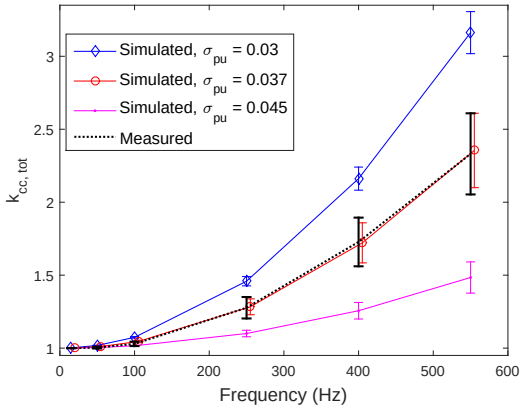

Fig. 11. Total circulating current factors calculated with the refined circuit model as a function of frequency. Slot permutations no longer assumed independent.

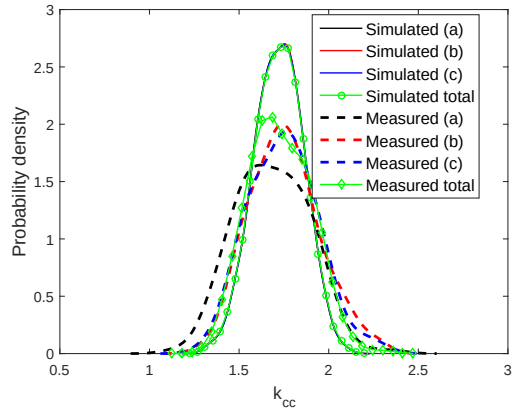

Fig. 12. Probability density functions of the circulating current factors at 450 Hz. The simulated results have been calculated by the analytical model with dependent permutations and $\sigma_{\text{pu}} = 0.037$. Factors for each phase (a,b,c) and the entire machine are shown.

As before, increasing σ_{pu} resulted in lower losses on average. This time however, the variance of $k_{\text{cc,tot}}$ peaked with $\sigma_{\text{pu}} = 0.037$, and decreased towards both ends of the simulated range. At the upper end of the range, the results approached the previously obtained ones. This is understandable, since uniformly permuting ($\sigma >> 1$) the strands would break all dependence between successive turns.

D. Predicted Full-Load Behaviour

Although the results obtained thus far are preliminary, some *predictive calculations* about the statistical properties at full-load could still be interesting. As no full-load measurement data was available, the following results have not been verified, and should be regarded with certain scepticism.

The simulations were repeated for a loaded machine supplied with a balanced sinusoidal 450 Hz voltage source. The slip was varied from no-load to standstill. To avoid the computational cost of modelling a solid rotor, only the circuit model

was utilized. The magnetizing and rotor branch impedances were calculated with FEM at the rated slip $s_{\mathrm{N}} = 0.007$. The rotor parameters were then scaled for different slips as shown in Fig. 13, with the method described in [39]. The strands were randomized in the previously described dependent fashion with a fixed $\sigma_{\mathrm{pu}} = 0.037$. A total of 10 000 machine samples were simulated, both at ambient and rated temperatures.

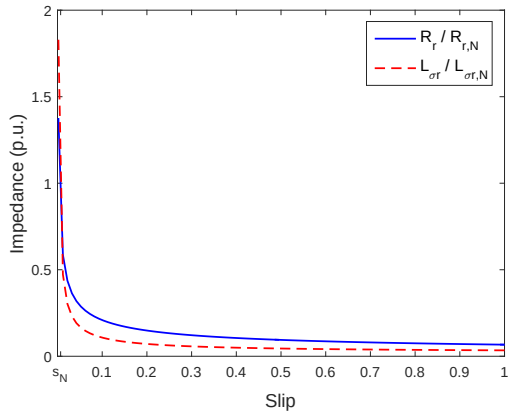

Fig. 13. Slip dependency of the rotor parameters, referred to the stator.

The circulating current factor as a function of slip can be seen in Fig. 14. Values corresponding to the simulated no-rotor test of Fig. 11 at 450 Hz have also been included for comparison. As expected, the results for a cold machine are close to the ones obtained without the rotor, and practically independent of the slip. At the rated temperature the values are somewhat lower, due to the increased resistances [38]. Nevertheless, the results suggest that the stator resistive losses at any load can be predicted from the locked-rotor test.

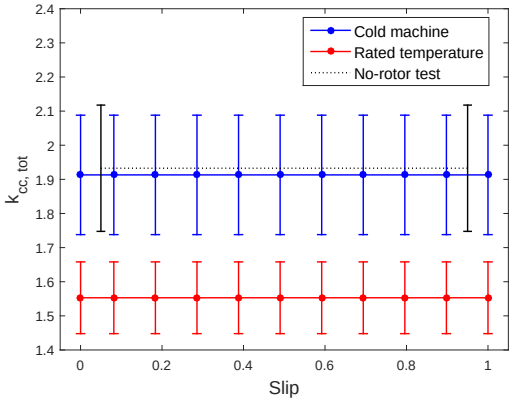

Fig. 14. The predicted circulating current factor as a function of slip at 450 Hz. Strands have been randomized in the dependent fashion with $\sigma_{\mathrm{pu}} = 0.0037$.

Fig. 15 shows the mean torque curve and standard deviations obtained from the MC analysis at rated temperature. The single-valued curve obtained from the conventional T equivalent circuit is also shown for comparison. It can be seen that randomizing the winding has little effect on the torque. This was expected, since the main flux was assumed to link all strands in one slot equally. Nevertheless, there seems to be a minor decrease in the maximum torque, probably due to the increase in the stator impedance. By contrast, the variation in the torque is extremely small – approximately 0.05 % at the rated slip and peaking at 0.23 % with $s = 5s_{\mathrm{N}}$.

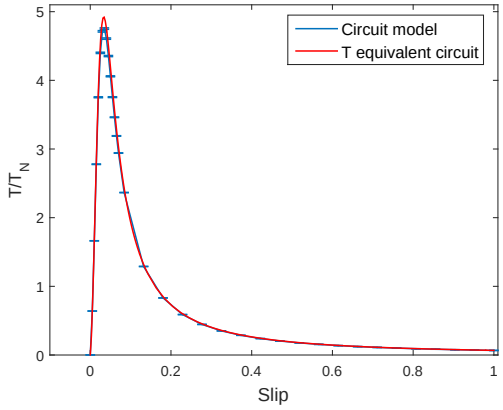

Fig. 15. Torque curves as a function of slip at 450 Hz, obtained from the T equivalent circuit and the proposed circuit model.

Yet another result of interest is the distribution of losses within one slot. Thus, individual strand losses were calculated at the rated slip and temperature for each MC sample. As an example, three randomly selected loss distributions in slot 1 are illustrated in Fig. 16. Relative values are shown, compared to the ideal situation of equal total current in each strand. It seems that any hot-spots are relatively few in number, but can have significantly higher losses in comparison.

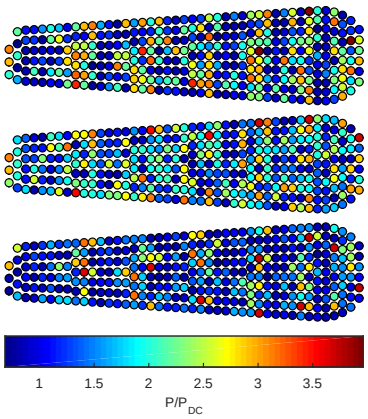

Fig. 16. Samples of the strand losses of slot 1 with randomized strand configurations.

Similarly, Fig. 17 shows the mean values of the individual strand losses in slot 1. As could be expected, the highest mean losses are concentrated near the inter-turn borders, especially on the slot-opening side of each turn [24]. However, in reality some mixing of strands could be expected on the boundary, decreasing the average losses in these areas. Furthermore, brief analysis revealed that the strand losses are practically uncorrelated with those of the neighbouring strands, with the Pearson's correlation coefficients r on the order of 0.1. Therefore, the worst hotspots *should* be physically separated,

although some further analysis is obviously required. Additionally, the multiphysics coupling between the uneven local heating and the strand resistances should be analysed.

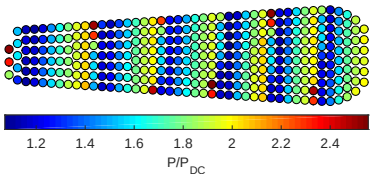

Fig. 17. Mean values of the strand losses of slot 1.

VII. Conclusion

Two efficient methods were proposed for analysis of circulating current losses in a stranded winding. Firstly, a circuit-based model was presented, based on the self and mutual inductances of the strands inside each slot. Also the rotor-side equivalent circuit was included, and practical implementation issues were discussed. Secondly, an efficient finite element formulation was proposed. The recently proposed non-conforming mesh approach [27] was improved by neglecting the skin and proximity effects, yielding very reasonable computation times.

Furthermore, an approach was proposed to model the random winding process. By randomly permuting the order of strands within a set of pre-defined positions, instead of fully modelling the packing process, the same pre-calculated inductances or FE mesh could be used for all simulations. This simplification should yield significant computation time savings and simplify the theoretical considerations included. Based on brief mathematical analysis, it should not present any large errors in the strand inductances. Finally, an ad-hoc algorithm was proposed to approximate normally distributed variations in strand positions.

The proposed methods were then compared to no-rotor test data of a large number of high-speed induction machines. Monte Carlo analysis was performed to model the statistical behaviour, with the slot packings assumed statistically independent. A good agreement of mean circulating current losses was easily obtained between both the circuit and FE methods, and the measurements. However, both methods predicted significantly smaller variances of losses compared to the measured data. Much better results were obtained by discarding the independence assumption, but more work would still be needed to obtain a perfect agreement.

Based on simulations, the analysed induction machines should exhibit proportionally slightly smaller circulating current losses at full load, compared to the no-rotor test set-up. However, the ratio between AC and DC resistive losses should be practically independent of the slip. Furthermore, the effect on machine torque should be minimal. Although winding hotspots could be expected, most of them should be isolated, with the neighbouring strands having significantly lower losses.

However, some further work should still be performed. The proposed circuit model should be more thoroughly validated at nominal machine operation, either against measurements or numerically. For the latter approach, some suitable model order reduction technique should probably be utilized to decrease the computational cost of modelling a solid rotor. Furthermore, the stochastic model of the strand packing process, i.e. the distribution of the random permutation matrices, could probably still be improved. Finally, multiphysic analysis of the thermal behaviour of the strands could be interesting.

Acknowledgment

Nicola Chiodetto would like to thank Prof. Nicola Bianchi for instructions and guidance. The research leading to these results has received funding from the European Research Council under the European Unions Seventh Framework Programme (FP7/2007-2013) / ERC Grant Agreement n. 339380.

Appendix A
Derivation of the Flux Density Coefficient

An expression for the coefficient k_B can be easily derived from the material presented in this paper, assuming that the magnetizing inductance L_m is known. Setting the rotor current to zero, the voltage vector over the magnetizing branch will be

$$\underline{u} = \mathrm{j}\omega L_\mathrm{m}\underline{i}_\mathrm{s}. \tag{35}$$

On the other hand, the same voltage can also be obtained by summing the voltages induced in all the strands in the machine, i.e. by combining (7), (15) and (16) to obtain

$$\underline{u} = \mathbf{P}_{\alpha\beta}\mathbf{L}_\mathrm{U}\sum_{k=1}^{Q_\mathrm{s}}\mathbf{C}_k^\mathrm{T}\mathrm{j}\omega r_\delta l_\mathrm{eff}\exp\left(\mathrm{j}\frac{2\pi}{Q_\mathrm{s}}k\right)\cdot\mathbb{1}_{N_\mathrm{strands}\times 1}\cdot k_\mathrm{B}\underline{i}_\mathrm{s}. \tag{36}$$

Here, the matrix

$$\mathbf{L}_\mathrm{U} = \frac{1}{2N_\mathrm{p}}\mathbf{I}_{3\times 3}\otimes\mathbb{1}_{1\times 2N_\mathrm{p}} \tag{37}$$

is used to calculate the phase voltages from the average voltage induced in the current loops. Strictly speaking, given the assumptions in this paper, the induced voltage should be equal for all parallel paths, but the averaging operation (37) is adopted for numerical stability.

Combining (35) and (36) and yields the desired expression

$$k_\mathrm{B} = \frac{\mathrm{j}\omega L_\mathrm{m}}{\mathrm{j}\omega r_\delta l_\mathrm{eff}\mathbf{P}_{\alpha\beta}\mathbf{L}_\mathrm{U}\left(\sum_{k=1}^{Q_\mathrm{s}}\mathbf{C}_k^\mathrm{T}\exp\left(\mathrm{j}\frac{2\pi}{Q_\mathrm{s}}k\right)\right)\cdot\mathbb{1}_{N_\mathrm{strands}\times 1}}. \tag{38}$$

Appendix B
Modelling Random Slot Packing

One of the most important assumptions of this paper is that the random packing of strands inside slots can be sufficiently modelled by randomly assigning the strands to pre-defined positions, rather than modelling the entire packing process. A brief justification for this assumption is presented here.

Let there be N strands inside one slot, and $\mathbf{x}_1^0,\ldots,\mathbf{x}_N^0$ be the strand center points in the *pre-defined* packing. Now,

consider an actual packing with the strands centered at $\mathbf{x}_1, \ldots, \mathbf{x}_N$. Re-number $\mathbf{x}^0$ so that the squared total distance

$$\sum_{k=1}^{N} \left\| \mathbf{x}_k^0 - \mathbf{x}_k \right\|^2 \tag{39}$$

is minimized – often equivalent to assigning index k to the point $\mathbf{x}^0$ closest to $\mathbf{x}_k$. Provided that $\mathbf{x}^0$ are reasonably distributed in the slot, and that the strand diameter is much smaller than the slot dimensions, $\|\mathbf{x}_k^0 - \mathbf{x}_k\|$ will be small for all k.

On the other hand, the self and mutual inductances of the strands in the actual packing can be written as

$$L_{ij} = L_{ij}^0 + \Delta_{ij}\left(\mathbf{x}_i - \mathbf{x}_i^0, \mathbf{x}_j - \mathbf{x}_j^0\right) \tag{40}$$

where L_{ij}^0 are the inductances of strands at the pre-defined positions. Δ_{ij} is an error function, with $\Delta_{ij} = 0$ for all $\mathbf{x}_i, \mathbf{x}_j = \mathbf{x}_i^0, \mathbf{x}_j^0$. Since the inductances – and by extension Δ – are continuous continuously dependent on the position within slot, $L_{ij} \approx L_{ij}^0$ since $\|\mathbf{x}_k^0 - \mathbf{x}_k\|$ are small.

Now, when comparing a large number of different packings, each L_{ij} may exhibit considerable variation due to the strands being in different positions in the slot. However, based on the above reasoning, in each case all L_{ij} can be closely approximated by the corresponding L_{ij}^0. In other words, the set of strand inductances with any strand packing can be approximated by the set of pre-calculated inductances L_{ij}^0, by a suitable permutation of the indices ij.

REFERENCES

[1] J. Lähteenmäki, "Design and voltage supply of high-speed induction machines," Ph.D. dissertation, Helsinki University of Technology, Espoo, Nov. 2002. [Online]. Available: http://lib.tkk.fi/Diss/2002/isbn951226224X/

[2] H. Khang and A. Arkkio, "Eddy-current loss modeling for a form-wound induction motor using circuit model," *IEEE Trans. Magn.*, vol. 48, no. 2, pp. 1059–1062, Feb 2012.

[3] M. Islam, J. Pippuri, J. Perho, and A. Arkkio, "Time-harmonic finite-element analysis of eddy currents in the form-wound stator winding of a cage induction motor," *IET Electric Power Applications*, vol. 1, no. 5, pp. 839–846, Sept 2007.

[4] M. Islam and A. Arkkio, "Time-stepping finite-element analysis of eddy currents in the form-wound stator winding of a cage induction motor supplied from a sinusoidal voltage source," *IET Electric Power Applications*, vol. 2, no. 4, pp. 256–265, July 2008.

[5] H. Khang, A. Arkkio, and J. Saari, "Loss minimization for form-wound stator winding of a high-speed induction motor," *IEEE Trans. Magn.*, vol. 48, no. 12, pp. 4874–4879, Dec 2012.

[6] M. Islam, H. Khang, A. Repo, and A. Arkkio, "Eddy-current loss and temperature rise in the form-wound stator winding of an inverter-fed cage induction motor," *IEEE Trans. Magn.*, vol. 46, no. 8, pp. 3413–3416, Aug 2010.

[7] M. Islam, "Finite-element analysis of eddy currents in the form-wound multi-conductor windings of electrical machines," Ph.D. dissertation, Aalto University, Espoo, Jan. 2010. [Online]. Available: http://lib.tkk.fi/Diss/2010/isbn9789522482556/

[8] Z. De Greve, O. Deblecker, J. Lobry, and J.-P. Keradec, "High-frequency multi-winding magnetic components: From numerical simulation to equivalent circuits with frequency-independent RL parameters," *IEEE Trans. Magn.*, vol. 50, no. 2, pp. 141–144, Feb 2014.

[9] J. Gyselinck, R. Sabariego, and P. Dular, "Time-domain homogenization of windings in 2-D finite element models," *IEEE Trans. Magn.*, vol. 43, no. 4, pp. 1297–1300, April 2007.

[10] R. Sabariego, P. Dular, and J. Gyselinck, "Time-domain homogenization of windings in 3-D finite element models," *IEEE Trans. Magn.*, vol. 44, no. 6, pp. 1302–1305, June 2008.

[11] J. Gyselinck, P. Dular, N. Sadowski, P. Kuo-Peng, and R. Sabariego, "Homogenization of form-wound windings in frequency and time domain finite-element modeling of electrical machines," *IEEE Trans. Magn.*, vol. 46, no. 8, pp. 2852–2855, Aug 2010.

[12] J. Gyselinck and P. Dular, "Frequency-domain homogenization of bundles of wires in 2-D magnetodynamic FE calculations," *IEEE Trans. Magn.*, vol. 41, no. 5, pp. 1416–1419, May 2005.

[13] J. Sibue, J. Ferrieux, G. Meunier, and R. Periot, "Modeling of losses and current density distribution in conductors of a large air-gap transformer using homogenization and 3-D FEM," *IEEE Trans. Magn.*, vol. 48, no. 2, pp. 763–766, Feb 2012.

[14] J.-R. Sibue, G. Meunier, J.-P. Ferrieux, J. Roudet, and R. Periot, "Modeling and computation of losses in conductors and magnetic cores of a large air gap transformer dedicated to contactless energy transfer," *IEEE Trans. Magn.*, vol. 49, no. 1, pp. 586–590, Jan 2013.

[15] G. Diaz and E. Mombello, "Semianalytic integral method for fast solution of current distribution in foil winding transformers," *IEEE Trans. Magn.*, vol. 51, no. 9, pp. 1–9, Sept 2015.

[16] Z. Pantic and S. Lukic, "Computationally-efficient, generalized expressions for the proximity-effect in multi-layer, multi-turn tubular coils for wireless power transfer systems," *IEEE Trans. Magn.*, vol. 49, no. 11, pp. 5404–5416, Nov 2013.

[17] R. Scapolan, A. Gagnoud, and Y. Terrail, "3-D multistrands inductor modeling: Influence of complex geometrical arrangements," *IEEE Trans. Magn.*, vol. 50, no. 2, pp. 949–952, Feb 2014.

[18] M. Spang and M. Albach, "Optimized winding layout for minimized proximity losses in coils with rod cores," *IEEE Trans. Magn.*, vol. 44, no. 7, pp. 1815–1821, July 2008.

[19] X. Dexin, Y. Xiuke, Y. Yingying, B. Baodong, and N. Takahashi, "Circulating current computation and transposition design for large current winding of transformer with multi-section strategy and hybrid optimal method," *IEEE Trans. Magn.*, vol. 36, no. 4, pp. 1014–1017, Jul 2000.

[20] B. Baodong, X. Dexin, C. Jiefan, and O. Mohammed, "Optimal transposition design of transformer windings by genetic algorithms," *IEEE Trans. Magn.*, vol. 31, no. 6, pp. 3572–3574, Nov 1995.

[21] M. Popescu and D. Dorrell, "Proximity losses in the windings of high speed brushless permanent magnet AC motors with single tooth windings and parallel paths," *IEEE Trans. Magn.*, vol. 49, no. 7, pp. 3913–3916, July 2013.

[22] X. Bian and Y. Liang, "Circuit network model of stator transposition bar in large generators and calculation of circulating current," *IEEE Trans. Ind. Electron.*, vol. PP, no. 99, pp. 1–1, 2014.

[23] J. Yoshida, N. Hino, K. Takahashi, A. Nakahara, A. Komura, and K. Hattori, "Calculation method of circulating current in parallel armature windings in consideration of magnetic circuit," in *2013 IEEE Power and Energy Society General Meeting (PES)*, July 2013, pp. 1–5.

[24] F. Jiancheng, L. Xiquan, B. Han, and K. Wang, "Analysis of circulating current loss for high-speed permanent magnet motor," *IEEE Trans. Magn.*, vol. 51, no. 1, pp. 1–13, Jan 2015.

[25] M. van der Geest, H. Polinder, J. Ferreira, and D. Zeilstra, "Current sharing analysis of parallel strands in low-voltage high-speed machines," *IEEE Trans. Ind. Electron.*, vol. 61, no. 6, pp. 3064–3070, June 2014.

[26] A. Lehikoinen and A. Arkkio, "Efficient finite element computation of circulating currents in thin parallel strands," in *International Conference on the Computation of Electromagnetic Fields (Compumag 2015)*, Montreal, Canada, Jul. 2015.

[27] ——, "Efficient finite element computation of circulating currents in thin parallel strands," *IEEE Trans. Magn.*, vol. PP, no. 99, pp. 1–1, 2015.

[28] A. Mesrobian and J. Holdrege, "Random wound versus form wound on low voltage synchronous generators," in *Petroleum and Chemical Industry Conference, 1990. Record of Conference Papers., Industry Applications Society 37th Annual*, Sep 1990, pp. 185–190.

[29] A. Thomas, Z. Zhu, and G. Jewell, "Proximity loss study in high speed flux-switching permanent magnet machine," *IEEE Trans. Magn.*, vol. 45, no. 10, pp. 4748–4751, Oct 2009.

[30] A. Tessarolo, "Leakage field analytical computation in semiclosed slots of unsaturated electric machines," *IEEE Trans. Energy Convers.*, vol. 30, no. 2, pp. 431–440, June 2015.

[31] J. Pyrhönen, T. Jokinen, and V. Hrabovcova, *Design of Rotating Electrical Machines*. West Sussex, UK: John Wiley & Sons, Ltd, 2008.

[32] A. Arkkio, "Analysis of induction motors based on the numerical solution of the magnetic field and circuit equations," Ph.D. dissertation, Helsinki University of Technology, Espoo, Finland, Dec. 1987. [Online]. Available: http://lib.tkk.fi/Diss/198X/isbn951226076X/isbn951226076X.pdf

[33] A.-K. Repo, P. Rasilo, A. Niemenmaa, and A. Arkkio, "Identification of electromagnetic torque model for induction machines with numerical magnetic field solution," *IEEE Trans. Magn.*, vol. 44, no. 6, pp. 1586–1589, June 2008.
[34] A. Tessarolo, F. Agnolet, F. Luise, and M. Mezzarobba, "Use of time-harmonic finite-element analysis to compute stator winding eddy-current losses due to rotor motion in surface permanent-magnet machines," *IEEE Trans. Energy Convers.*, vol. 27, no. 3, pp. 670–679, Sept 2012.
[35] A. Lehikoinen, "Spectral stochastic finite element method for electromagnetic problems with random geometry," *Electrical, Control and Communication Engineering*, vol. 6, pp. 5–12, 2014.
[36] E. Lantto, A. Arkkio, M. Antila, K. Pokki, and A. Simon, "Electromagnetic forces caused by cage induction motor," in *Proceedings of the 7th International Symposium on Magnetic Bearings*, Zurich, Switzerland, Jul. 2000, pp. 589–594.
[37] N. Chiodetto, "Monte Carlo analysis of circulating currents in random wound electrical machines," Master's thesis, Aalto University, Espoo, Finland, 2015.
[38] H. Hämäläinen, J. Pyrhönen, and J. Nerg, "AC resistance factor in one-layer form-wound winding used in rotating electrical machines," *IEEE Trans. Magn.*, vol. 49, no. 6, pp. 2967–2973, June 2013.
[39] J. Gieras and J. Saari, "Performance calculation for a high-speed solid-rotor induction motor," *IEEE Trans. Ind. Electron.*, vol. 59, no. 6, pp. 2689–2700, June 2012.

Antti Lehikoinen was born in December 1988. He received his Bachelor's degree in Science (Technology) in 2012 from the Aalto University School of Electrical Engineering, and the M.Sc. degree a year later from the same institute, with a major in electromechanics.

He is currently making his doctoral thesis in the School of Electrical Engineering, Espoo, Finland. He is mainly focusing on efficient finite element modelling of multi-conductor windings, and the stochastic properties of circulating current losses in random-wound machines.

Nicola Chiodetto was born in December 1990. He received his Bachelor's degree in Energy Engineering in 2012 from the University of Padova. He has worked towards his M.Sc. degree both in Italy, at University of Padova, and USA, Boston University. He performed his Master's Thesis at Aalto University and he received his M.Sc. degree in Electrical Engineering in 2015 from University of Padova.

He is currently working toward the Ph.D. degree at the University of Padova. His research is focused on design, optimization and control of high speed permanent magnet generators.

Antero Arkkio was born in Vehkalahti, Finland in 1955. He received his M.Sc. (Tech.) and D.Sc. (Tech.) degrees from Helsinki University of Technology in 1980 and 1988. Currently he is a Professor of Electrical Engineering at Aalto University. His research interests deal with modeling, design, and measurement of electrical machines.

Anouar Belahcen (M13,SM'15) was born in Morocco, in 1963. He received the B.Sc. degree in physics from the University Sidi Mohamed Ben Abdellah, Fes, Morocco, in 1988 and the M.Sc. (Tech.) and Doctor (Tech.) degrees from Helsinki University of Technology, Finland, in 1998, and 2004, respectively. From 2008 to 2013, he has been working as Adjunct Professor in the field of coupled problems and material modeling at Aalto University, Finland. Since 2011 he is Professor of electrical machines at Tallinn University of Technology, Estonia and in 2013 he became Professor of Energy and Power at Aalto University. His research interest are numerical modeling of electrical machines, especially magnetic material modeling, coupled magnetic and mechanical problems, magnetic forces, and magnetostriction.